

## Depassivation kinetics in crystalline silicon nanoparticles

R. N. Pereira,<sup>1,2</sup> S. Niesar,<sup>2</sup> H. Wiggers,<sup>3</sup> M. S. Brandt,<sup>2</sup> and M. S. Stutzmann<sup>2</sup>

<sup>1</sup>*Department of Physics and I3N, University of Aveiro, Campus Universitário de Santiago, 3810-193 Aveiro, Portugal*

<sup>2</sup>*Walter Schottky Institut, Technische Universität München, Am Coulombwall 4, 85748 Garching, Germany*

<sup>3</sup>*Institut für Verbrennung und Gasdynamik and CENIDE, Universität Duisburg-Essen, 47048 Duisburg, Germany*

(Received 24 May 2013; published 22 October 2013)

The formation of silicon dangling bond (Si-db) defects in crystalline silicon nanoparticles (Si-NPs) is studied by electron paramagnetic resonance combined with vacuum-annealing experiments. The kinetics of Si-db formation due to H desorption is found to be reliably described by a first-order-rate thermal model with a mean activation energy  $E_d = 2.25$  eV and a spread  $\sigma_{E_d} = 0.28$  eV in the activation energy distribution. These values deviate from those reported in previous studies of other Si-based materials, which is attributed to the presence of different interfacial hydrides  $\text{Si}_{4-n}-\text{Si}-\text{H}_n$ . Hence, the generation Si-db defects in Si-NPs initiates at a much lower temperature than one would expect based on the previously reported kinetics parameters. Unlike the case of planar Si/SiO<sub>2</sub> interfaces, no permanent interface degradation is observed upon annealing of Si-NPs at temperatures  $\gtrsim 600$  °C. This, together with the observation of an interfacial Si-db density similar to that typically incorporated in high quality thermally-grown SiO<sub>2</sub> on bulk silicon, indicates the formation of a rather relaxed and thermally stable surface oxide shell during natural oxidation of Si-NPs.

DOI: [10.1103/PhysRevB.88.155430](https://doi.org/10.1103/PhysRevB.88.155430)

PACS number(s): 81.07.Bc, 61.72.Cc, 81.65.Rv, 76.30.Mi

Low-cost processing as well as promising physical properties, such as wavelength tunable light emission and absorption, are driving intensive research on semiconductor nanoparticles for use in new applications such as green energy and biomedical treatments.<sup>1–9</sup> In particular, crystalline silicon nanoparticles (Si-NPs) offer many advantages when compared to NPs of other semiconductors; e.g., they are made of an abundant, environmentally inert, and biocompatible element.<sup>10</sup> The recently developed capability of producing macroscopic amounts of high quality crystalline Si-NPs using gas phase plasma synthesis (e.g., Refs. 11 and 12) has opened up the route for new applications such as cost-efficient large area electronics using printable NP-inks,<sup>13–15</sup> thermoelectrics,<sup>16,17</sup> solar energy to electricity conversion,<sup>18–20</sup> and light emission.<sup>21,22</sup> Several studies have been reported in recent years focusing on basic characteristics of these gas-phase grown Si-NPs including light emission properties,<sup>12,23</sup> electronic doping,<sup>24–27</sup> and defects.<sup>28,29</sup> Si-NPs are prone to oxidation upon storage at room temperature and ambient atmosphere, which results in the formation of a thin native oxide shell.<sup>15,30</sup> Due to the mismatch between crystalline silicon and the amorphous surface oxide shell, a sizable number of the silicon atoms at the Si/SiO<sub>2</sub> interface establish covalent bonding to only three other silicon atoms. Some of these interfacial Si atoms comprise an  $sp^3$ -like dangling bond (db), forming paramagnetic point defects symbolized as  $\text{Si}_3\equiv\text{Si}^\bullet$ , where the dot represents the db.<sup>31</sup> Another significant fraction of the interfacial silicon atoms, however, become passivated as a result of Si–H bond formation at the Si/SiO<sub>2</sub> interface during natural oxidation.<sup>32,33</sup> The thermal stability of this interfacial H passivation is a rather important issue from a technology viewpoint, in particular since fabrication of devices based on Si-NPs may require thermal treatments,<sup>10,16,19,20</sup> which potentially promote the breaking of interfacial Si–H bonds and consequently generate Si-db defects that have an adverse impact on applications. For instance, these act as recombination and trapping centers for electrons and holes moving

across Si-NP thin films,<sup>28,32</sup> strongly decrease the efficiency of electronic impurity doping,<sup>24</sup> and are associated with the degradation of light emission from confined excitons.<sup>12,34</sup>

In this study, the kinetics of Si-db formation due to atomic hydrogen desorption from interfacial Si–H bonds in crystalline Si-NPs is studied by electron paramagnetic resonance (EPR) combined with isochronal vacuum-annealing experiments. Our annealing data is quantitatively described using a model that takes into account a spread in the activation energy for thermal Si–H bond dissociation. The results obtained in our experiments for Si-NPs are confronted with those reported in previous studies of defect formation at flat Si/SiO<sub>2</sub> interfaces and in Si nanocrystals embedded in amorphous SiO<sub>2</sub> (*a*-SiO<sub>2</sub>). Moreover, the inherent defect density and thermal stability of the native Si/SiO<sub>2</sub> interface in Si-NPs are compared with literature data of planar Si/SiO<sub>2</sub> interfaces.

The Si-NPs investigated were synthesized in a low pressure microwave reactor by plasma-induced decomposition of silane.<sup>12</sup> This method yields macroscopic amounts of spherical crystalline Si-NPs with a surface oxide layer formed after exposure to air with a thickness in the range of  $1.4 \pm 0.2$  nm, as determined by high-resolution transmission electron microscopy.<sup>15</sup> The Si-NPs investigated here have a log-normal size distribution with a mean diameter of 15.6 nm, obtained from the Brunauer-Emmett-Teller method,<sup>35</sup> and a standard deviation of the diameter natural logarithm of typically  $\sigma = 0.40$ .<sup>36</sup> We refer to these Si-NPs, surrounded by a native oxide shell formed by storing at room temperature and ambient atmosphere and measured without further treatment after synthesis, as *as-grown* Si-NPs. Isochronal thermal treatments of 2 h duration were performed in an evacuated quartz tube with a base pressure of  $<10^{-7}$  mbar that was surrounded by a resistively-heated tube oven. For each thermal treatment, a sample of Si-NPs was prepared by inserting 2–3 mg of *as-grown* Si-NP powder into a suprasil quartz EPR sample tube. EPR measurements of these samples were performed

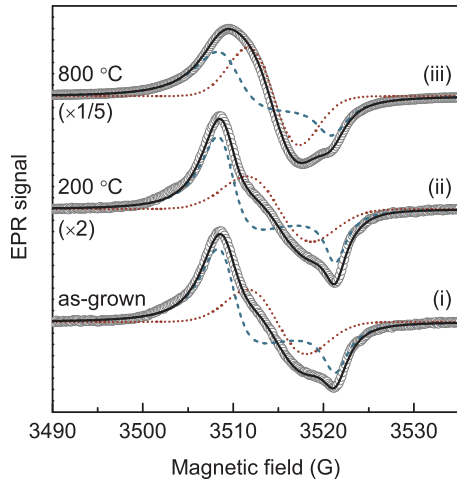


FIG. 1. (Color online) EPR spectra of as-grown Si-NPs (i) and Si-NPs annealed at 200 °C (ii) and 800 °C (iii). Open circles correspond to experimental data and solid curves represent computer simulations, taking into account a powder pattern of axial symmetry due to  $P_b^{NP}$  dangling bonds (dashed curves) and an isotropic resonance due to  $D$  defects (dotted curves).

at room temperature with a conventional continuous-wave X-band spectrometer using a lock-in amplifier and a  $TM_{110}$  cavity. Calibrations of  $g$  values and EPR intensity were done by comparison with the signal of a 2,2-diphenyl-1-picrylhydrazyl reference sample measured at room temperature. Under our experimental conditions, the accuracies of the absolute spin density and  $g$  values are better than 30% and 0.0005, respectively.

The EPR spectrum recorded for as-grown Si-NPs is shown in curve (i) of Fig. 1. This spectrum exhibits the resonance structure typically observed for gas-phase grown Si-NPs. It originates from two types of defects present simultaneously,<sup>31,37</sup> i.e., silicon dangling bonds (Si-dbs) at the interface between the NPs crystalline silicon core and the surface oxide shell (denoted  $P_b^{NP}$  defects) and Si-dbs in a disordered environment, referred to as  $D$  defects.<sup>31,37</sup> A similar band due to Si-dbs is also observed for Si-NPs annealed at temperatures in the range 150–800 °C. All these spectra can be well described taking into account an axially symmetric powder pattern of Lorentzian lines, whose linewidths increase linearly from the direction parallel to the symmetry axis to the perpendicular direction, and an isotropic line with Gaussian shape. Experimental spectra and corresponding numerical simulations taking into account these two spectral components are also shown in Fig. 1 for the cases of samples annealed at 200 and 800 °C. Figure 2(a) shows the values obtained from the numerical fitting for the  $g$  values  $g_{\perp}$  and  $g_{\parallel}$  of the axial spectral component and  $g_D$  of the isotropic component for different vacuum-annealing temperatures  $T_{\text{anneal}}$ . No significant variation of the parameters of  $g_{\perp}$ ,  $g_{\parallel}$ ,  $g_D$  is obtained with respect to values extracted for the spectrum of the as-grown Si-NPs (indicated at  $T_{\text{anneal}} = 50$  °C). This demonstrates that the axial and isotropic spectral components of the spectra of the annealed samples also correspond to  $P_b^{NP}$  and  $D$  defects, respectively. The dependence of the total Si-db density on the vacuum-annealing temperature is

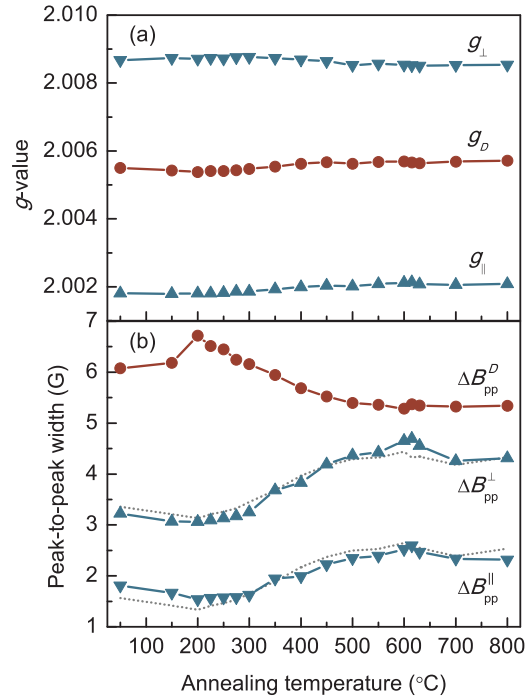


FIG. 2. (Color online) Variation of  $g$  values (a) and peak-to-peak linewidths (b) of the axial ( $P_b^{NP}$ ) and isotropic ( $D$ ) EPR spectral components as a function of vacuum-annealing temperature.

shown in Fig. 3, obtained by numerical double integration of the simulated spectra (solid lines in Fig. 1). As can be seen, the Si-db density decreases with increasing vacuum-annealing temperature for  $T_{\text{anneal}} \leq 200$  °C, in agreement with previous observations.<sup>28</sup> However, a strong increase of the density of Si-dbs is observed for vacuum-annealing temperatures above 200 °C, followed by a saturation at about  $6 \times 10^{12}$  cm<sup>-2</sup> at  $T_{\text{anneal}} \simeq 500$  °C. In this temperature interval, the relative density ratio of  $P_b^{NP}$  and  $D$  defects ( $[P_b^{NP}]/[D]$ ) remains unchanged within experimental accuracy (inset of Fig. 3).

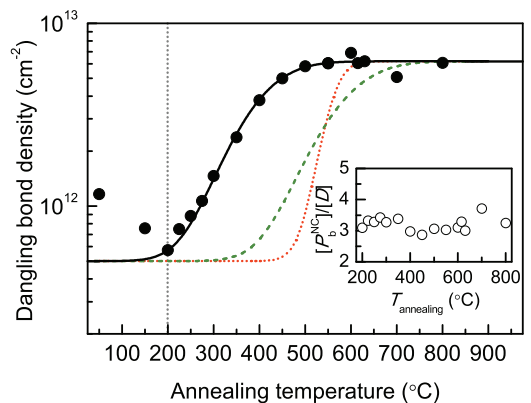


FIG. 3. (Color online) Experimental dependence of Si-db defect density as a function of vacuum-annealing temperature (solid dots). The solid line represents the least-square fit of the model described in the text. Dotted and dashed lines correspond to dependencies calculated with the same model using reaction-rate parameters reported previously for flat Si/SiO<sub>2</sub> interface and Si-NCs in  $\alpha$ -SiO<sub>2</sub>.<sup>40,44</sup>

This indicates that the vacuum-annealing behavior of the  $P_b^{\text{NP}}$  and  $D$  dangling bonds is identical. It is worth noting that the density of interfacial Si-db defects inherently present in the surface-oxidized Si-NPs ( $\sim 6 \times 10^{12} \text{ cm}^{-2}$ ) is very similar to that typically present at the interface between high quality thermally-grown (800–950 °C)  $\text{SiO}_2$  and bulk silicon ( $\sim 5 \times 10^{12} \text{ cm}^{-2}$ ).<sup>38–40</sup> This indicates that surface oxidation of the Si-NPs at room temperature in air readily results in a high quality interface between the NPs crystalline core and the surface oxide shell. We should note that for the case of bulk silicon low interfacial defect densities in the range of  $5 \times 10^{12} \text{ cm}^{-2}$  are only attained in high temperature oxidation conditions ( $\gtrsim 800$  °C) and that oxidation at room temperature results in a considerably more defective interface ( $[\text{Si-db}] \sim 20 \times 10^{12} \text{ cm}^{-2}$ ).<sup>38</sup> Stress due to the mismatch between Si and  $\text{SiO}_2$  is broadly accepted as the reason for the appearance of Si-dbs in Si/ $\text{SiO}_2$  interfaces.<sup>38–41</sup> A linear correlation has been found between stress and the concentration of Si-db defects.<sup>38</sup> For oxidation above 800 °C, structure relaxation of the  $\text{SiO}_2$  reduces the need for generation Si-dbs to account for lattice mismatch. Therefore, the relatively low density of Si-dbs found in our Si-NPs points out to the formation of a readily relaxed surface oxide shell during natural oxidation.

Following earlier studies of Si-dbs at flat (111)Si/ $\text{SiO}_2$  interfaces, generally known as  $P_b$  centers,<sup>41–43</sup> we consider that the generation of Si-dbs in our Si-NPs is simply governed by the differential rate equation  $d[\text{Si-db}]/dt = k_d N_0 - [\text{Si-db}]$ , where  $t$  is time,  $k_d$  is the rate constant, and  $N_0$  is the maximum density of EPR-active unpassivated Si-db centers, with the general solution

$$[\text{Si-db}](t) = N_0 - \{N_0 - [\text{Si-db}](0)\} \times \exp\{-k_d t\}. \quad (1)$$

The temperature dependence of the rate constant is given by the Arrhenius equation  $k_d = k_{d0} \exp(-E_d/kT)$ .<sup>42,43</sup> Here,  $k_{d0}$  is the rate constant at  $T = 0$  K,  $E_d$  is the activation energy for Si-db formation, e.g., by Si–H dissociation,  $k$  is the Boltzmann constant, and  $T$  is the temperature. The kinetics of generation of  $P_b$  centers at flat Si/ $\text{SiO}_2$  interfaces was found reliably described taking into account a spread in the activation energy  $E_d$ .<sup>40,41</sup> By convoluting a Gaussian spread in  $E_d$  with Eq. (1),<sup>40</sup> the following expression is obtained:

$$[\text{Si-db}](t) = N_0 - \frac{\{N_0 - [\text{Si-db}](0)\}}{\sqrt{2\pi}\sigma_{E_d}} \int_0^\infty \exp\left[-\frac{(E - E_d)^2}{2\sigma_{E_d}^2}\right] \times \exp\left[-tk_{d0} \exp\left(\frac{-E}{kT}\right)\right] dE, \quad (2)$$

where  $\sigma_{E_d}$  is the parameter quantifying the spread in activation energy and  $E_d$  represents the mean activation energy. Using Eq. (2), we can now describe the increase of  $[\text{Si-db}]$  with  $T_{\text{anneal}}$  observed in our isochronal vacuum-annealing experiments quantitatively. Here,  $N_0 = 6.2 \times 10^{12} \text{ cm}^{-2}$  is the experimentally observed saturation value of  $[\text{Si-db}]$ , i.e.,  $[\text{Si-db}]$  for  $T_{\text{anneal}} = 800$  °C,  $[\text{Si-db}](0) = 5 \times 10^{11} \text{ cm}^{-2}$  is the initial Si-db density, and  $k_{d0} = 1.6 \times 10^{13} \text{ s}^{-1}$  agrees with the rate constant prefactor obtained previously for  $P_b$  centers at a flat (111)Si/ $\text{SiO}_2$  interface.<sup>40</sup> The solid line in Fig. 3 shows the dependence of  $[\text{Si-db}]$  on  $T_{\text{anneal}}$  obtained by fitting Eq. (2) to the experimental data, for  $T_{\text{anneal}} \geq 200$  °C, leaving  $E_d$  and

TABLE I. Kinetic parameters for thermal generation of paramagnetic Si-db centers in different silicon-based materials.

Reference	$E_d$ (eV)	$\sigma_{E_d}$ (eV)	Material
This work	$2.25 \pm 0.06$	$0.28 \pm 0.04$	Si-NPs
Ref. 40	$2.83 \pm 0.02$	$0.08 \pm 0.03$	planar (111)Si/ $\text{SiO}_2$
Ref. 44	$2.90 \pm 0.05$	$0.29 \pm 0.03$	Si-NCs in $\alpha$ - $\text{SiO}_2$

$\sigma_{E_d}$  as fitting parameters. As can be seen, a good agreement between experimental and simulated data is obtained. From this fit we extract the values  $E_d = 2.25 \pm 0.06$  eV and  $\sigma_{E_d} = 0.28 \pm 0.04$  eV. Table I compares these values with those reported previously for the generation of  $P_b$  centers at a flat (111)Si/ $\text{SiO}_2$  interface and of photoluminescence-quenching defects in Si nanocrystals (Si-NCs) embedded in  $\alpha$ - $\text{SiO}_2$ .<sup>40,44</sup> The dotted and dashed lines shown in Fig. 3 represent the vacuum-annealing dependence calculated with the reaction-rate parameters  $E_d$  and  $\sigma_{E_d}$  values obtained in these latter studies.<sup>40,44</sup> The numerical differences observed between the kinetics parameters obtained in our work and those reported previously result in the important consequence that the generation Si-db defects initiate at a much lower temperature than one would expect based on the previously reported kinetics parameters. Namely, while a 2 hour annealing at 400 °C would expectedly result in a minute generation of Si-dbs based on the parameters reported for (111)Si/ $\text{SiO}_2$  and Si-NCs in  $\alpha$ - $\text{SiO}_2$ , in our experiments the same annealing leads to an almost completed generation of Si-dbs. The values reported for  $P_b$  centers at (111)Si/ $\text{SiO}_2$  interfaces were obtained from directly monitoring the vacuum-annealing behavior of the density of  $P_b$  centers using EPR,<sup>40</sup> similar to our experiments, whereas the values for Si-NCs in  $\alpha$ - $\text{SiO}_2$  were derived from the vacuum-annealing behavior of luminescence-quenching defects measured indirectly with time-resolved photoluminescence (PL) spectroscopy.<sup>44</sup>

In earlier investigations,<sup>40,44,45</sup> the generation of defects during vacuum annealing, either at the (111)Si/ $\text{SiO}_2$  interface or in Si-NCs embedded in  $\alpha$ - $\text{SiO}_2$ , was attributed to the conversion of Si-dbs from the H-passivated state ( $\text{Si}_3 \equiv \text{Si}-\text{H}$ ) to the paramagnetic state ( $\text{Si}_3 \equiv \text{Si}^\bullet$ ) by desorption of atomic hydrogen from Si–H bonds. In such a case,  $E_d$  and  $k_d$  are the activation energy and rate constant of the atomic hydrogen dissociation. The fact that the values of  $E_d$  obtained for defect generation at (111)Si/ $\text{SiO}_2$  interface ( $E_d = 2.83$  eV) and in Si-NCs embedded in  $\alpha$ - $\text{SiO}_2$  ( $E_d = 2.90$  eV) agreed reasonably well indicated that the same reaction is involved in both cases.<sup>44</sup>

The annealing-induced generation of paramagnetic Si-dbs observed in our experiments should therefore also result from dissociation of atomic hydrogen from Si–H bonds. This is corroborated by temperature-programmed desorption (TPD) experiments carried out with a linear temperature ramp using Si-NPs similar to those studied in the present work,<sup>33</sup> where desorption of atomic hydrogen has been observed in the temperature range 250–550 °C, the same temperature range where we observe the generation of Si-db centers. However, the activation energy  $E_d = 2.25$  eV extracted from our isochronal vacuum-annealing data is significantly lower than the values  $E_d = 2.83$  and 2.90 eV reported in the studies mentioned

above. This indicates that distinct Si–H hydride species are involved in our case. In the previous experiments of flat Si/SiO<sub>2</sub> interfaces and Si-NCs in *a*-SiO<sub>2</sub>, the initial interfacial Si–H bonds have been mainly in the form of monohydrides Si<sub>3</sub>≡Si–H.<sup>40,44</sup> From Fourier-transform infrared spectroscopy data,<sup>32,33</sup> we know that along with monohydrides also dihydride Si<sub>2</sub>=Si=H<sub>2</sub> species are present in our Si-NPs. For the case of silicon surfaces, it is known that the activation energy for hydrogen desorption from surface dihydrides is lower than from surface monohydrides.<sup>45–48</sup> For example for the flat (100)Si surface, activation energies of 1.88 and 2.52 eV have been obtained for hydrogen desorption from surface dihydrides and monohydrides, respectively.<sup>48</sup> Other studies also report values of 2.04 and 2.43 eV, respectively, for the same type of surface.<sup>47</sup> These values are found to be 2.16 and 2.58 eV, respectively, for the case of the (113)Si surface.<sup>46</sup> For porous silicon surfaces, predominantly of (100)Si type, corresponding values of 1.86 and 2.82 eV, respectively, have been reported.<sup>45</sup> Thus, it is reasonable to assume that the activation energy for hydrogen desorption from Si<sub>2</sub>=Si=H<sub>2</sub> at Si/SiO<sub>2</sub> interface in our Si-NPs is lower than from Si<sub>3</sub>≡Si–H.<sup>46,49</sup> Therefore, in our case the Si-dbs are likely to be formed by dissociation of atomic hydrogen from Si–H bonds in both monohydride Si<sub>3</sub>≡Si–H and dihydride Si<sub>2</sub>=Si=H<sub>2</sub> configurations, which results in a lower mean activation energy  $E_d$  with respect to the previous studies where Si–H bonds were present uniquely in monohydrides.

We also find a difference between the value of activation energy spread  $\sigma_{Ed}$  reported for paramagnetic Si-db generation at flat Si/SiO<sub>2</sub> interfaces ( $\sigma_{Ed} = 0.08$  eV) and the value obtained in our study ( $\sigma_{Ed} = 0.29$  eV). For flat Si/SiO<sub>2</sub> interfaces,<sup>40,50</sup> it has been concluded that the spread in  $E_d$  results from a nonuniformity in the Si-db defects correlated with interface stress. Variations in the local geometry of Si–H bonds in the ensemble of interfacial monohydrides Si<sub>3</sub>≡Si–H result in a spread in bond strength via orbital rearrangements. Thus, in the reports on flat Si/SiO<sub>2</sub> interfaces,<sup>40,50</sup> the spread  $\sigma_{Ed}$  is mainly stress induced. The existence of a spread in  $E_d$  for the flat Si/SiO<sub>2</sub> interface is evidenced also by the fact that the  $P_b$  defect energy levels in the band gap display a significant distribution.<sup>51</sup> In our Si-NPs, a much larger spread in activation energies, associated with a broader range of Si–H bond strengths, is observed because Si–H bonds involved in the hydrogen dissociation reaction are both in the monohydride and in the dihydride configuration, which have sizably different bond strengths.<sup>45–48</sup> The existence of different facets in the nanocrystallites, which results in different microscopic environments, may also contribute to the observed spread in our Si-NPs. A higher value of  $\sigma_{Ed}$ , when compared to that reported for flat Si/SiO<sub>2</sub> interfaces, was also obtained for defect generation in Si-NCs in *a*-SiO<sub>2</sub>; see Table I.<sup>44</sup> However, the main contribution to the spread in this case varies from that of our Si-NPs. The large value of  $\sigma_{Ed}$  was suggested to result from differences in geometry of the spherical silicon/oxide interface of Si-NCs in *a*-SiO<sub>2</sub> with respect to the flat (111)Si/SiO<sub>2</sub> interface studied by Stesmans.<sup>44</sup> It was also suggested that the differences in  $\sigma_{Ed}$  could as well result from the fact that in the time-resolved PL measurements a wider range of defects may be monitored when compared to the EPR measurements performed for the

case of (111)Si/SiO<sub>2</sub> interfaces.<sup>44</sup> In the EPR experiments, only the paramagnetic Si-dbs centers are detected, whereas in the PL experiments all PL-quenching defects are monitored, resulting in a larger spread  $\sigma_{Ed}$ .<sup>44</sup>

As can be seen in Fig. 2(b), the EPR peak-to-peak linewidths  $\Delta B_{pp}^{\perp}$  and  $\Delta B_{pp}^{\parallel}$  associated with the  $P_b^{\text{NP}}$  dangling bonds vary with annealing temperature. Previous studies carried out on different flat Si/SiO<sub>2</sub> interfaces have concluded that the EPR linewidths of  $P_b$  centers consist mainly of three superimposed contributions: (i) a component due to strain-induced distributions of  $g_{\perp}$  and  $g_{\parallel}$ , (ii) a component due to dipolar broadening, resulting from dipole-dipole interactions among the unpaired electrons, and (iii) a component due to unresolved <sup>29</sup>Si superhyperfine interactions.<sup>52,53</sup> The widths  $\Delta B_{pp}^{\perp}$  and  $\Delta B_{pp}^{\parallel}$  display similar dependencies with annealing temperature [see Fig. 2(b)], and thus, the origin of the changes is most probably the same. If these changes would result from variations in the strain-induced component (i), these should be much stronger for  $\Delta B_{pp}^{\perp}$  than for  $\Delta B_{pp}^{\parallel}$  because  $g_{\perp}$  is much more sensitive to strain than  $g_{\parallel}$ ,<sup>52</sup> which is in clear contrast with our observations. Therefore, we can discard effect (i) as the one responsible for the linewidth variation. The dipolar broadening component (ii) is expected to increase when the dangling bond density increases, following a square-root dependence  $\Delta B_{pp}^{\perp,\parallel} \propto \sqrt{[\text{Si-db}]}$ .<sup>54</sup> The dotted lines in Fig. 2(b) represent such a dependence taking into account the values of [Si-db] given in Fig. 3. As can be seen, a reasonable agreement between the square-root dependence and experimental data is obtained, indicating that the changes in  $\Delta B_{pp}^{\perp}$  and  $\Delta B_{pp}^{\parallel}$  can be accounted for by variations in the dipole-dipole interaction.

Another noteworthy difference between the Si-NPs and planar Si/SiO<sub>2</sub> interfaces is found. In the case of planar Si/SiO<sub>2</sub> interfaces, vacuum annealing at temperatures higher than ~640 °C, i.e., above the temperature at which all H passivation is removed, results in an irreversible generation of Si-db defects.<sup>39,40</sup> This contrasts with our observations for Si-NPs, where the defect density measured in the annealing temperature range 600 to 800 °C is rather constant. The permanent degradation of planar Si/SiO<sub>2</sub> interfaces at annealing temperatures  $\gtrsim 640$  °C has been associated to interfacial SiO extraction preferentially at steps.<sup>39</sup> This leads to a reduction of the interfacial step density and formation of larger terraces, leaving less room for interfacial adaptation, which is accounted for by formation of additional Si-db defects.<sup>39</sup> The rather stable density of Si-dbs in Si-NPs for annealing temperatures above 600 °C should therefore be due to the spherical nature of the Si/SiO<sub>2</sub> interface, where the formation of large terraces is not possible. In this case, the release of interfacial SiO from steps is unfavored and the inherently curved, steplike interface provides the required interfacial adaptation. This also agrees with the conclusion put forward above that during natural oxidation of Si-NPs a quite relaxed surface oxide shell is formed, resulting in a relatively low incorporation of Si-dbs.

In summary, we have studied the formation Si-dbs resulting from thermally-induced H desorption in naturally-oxidized Si-NPs. We find that the density of interfacial Si-db defects present in the Si-NPs with a native oxide shell is very

similar to that typically incorporated in high quality, thermally-grown SiO<sub>2</sub> on bulk silicon, indicating the formation of a readily relaxed surface oxide shell during natural oxidation of Si-NPs. The kinetics of Si-db formation is found to be reliably described by a first-order-rate thermal model with a mean activation energy  $E_d = 2.25$  eV and with an associated Gaussian spread  $\sigma_{E_d} = 0.28$  eV. The observed deviations in the reaction-rate parameters obtained for Si-NPs from values reported in previous studies of other Si-based materials is attributed to the presence of interfacial hydrides Si<sub>4-n</sub>-Si-H<sub>n</sub> with different  $n$ . These deviations have the consequence that the generation Si-db defects in the Si-NPs initiates at a much lower temperature than one would expect based on the previously reported kinetics parameters. Unlike the case

of planar Si/SiO<sub>2</sub> interfaces, no permanent degradation of the interface is observed upon high temperature ( $\gtrsim 600$  °C) annealing of Si-NPs. This is possibly due to their inherently curved, steplike interface where reduction of interfacial step density, which is energetically favored in planar Si/SiO<sub>2</sub>, is not possible.

This work was funded by FCT via Projects No. PTDC/280/FIS/112885/2009, No. RECI/FIS-NAN/0183/2012, and No. PEst-C/CTM/LA0025/2011, by I3N via the HybridSolar Project, by CRUP-DAAD via the Acção Integrada Luso-Alemã A-22/09, and by DFG via Projects No. SFB 631 C3 and No. GK 1240.

- <sup>1</sup>N. Gaponik, S. G. Hickey, D. Dorfs, A. L. Rogach, and A. Eychmüller, *Small* **6**, 1364 (2010).
- <sup>2</sup>H. Wei, H. Zhang, H. Sun, and B. Yang, *Nano Today* **7**, 316 (2012).
- <sup>3</sup>E. Muro, A. Fragola, T. Pons, N. Lequeux, A. Ioannou, P. Skourides, and B. Dubertret, *Small* **8**, 1029 (2012).
- <sup>4</sup>M. D. Regulacio and M.-Y. Han, *Acc. Chem. Res.* **43**, 621 (2010).
- <sup>5</sup>V. M. Huxter and G. D. Scholes, *J. Nanophotonics* **3**, 032504 (2009).
- <sup>6</sup>P. Reiss, M. Protière, and L. Li, *Small* **5**, 154 (2009).
- <sup>7</sup>P. V. Kamat, *J. Phys. Chem. C* **112**, 18737 (2008).
- <sup>8</sup>N. Ma, G. Tikhomirov, and S. O. Kelley, *Acc. Chem. Res.* **43**, 173 (2010).
- <sup>9</sup>Q. Dai, C. E. Duty, and M. Z. Hu, *Small* **6**, 1577 (2010).
- <sup>10</sup>L. Pavesi and R. Turan, *Silicon Nanocrystals: Fundamentals, Synthesis and Applications* (WILEY-VCH Verlag GmbH & Co. KGaA, Weinheim, Germany, 2010).
- <sup>11</sup>L. Mangolini and U. Kortshagen, *Adv. Mater.* **19**, 2513 (2007).
- <sup>12</sup>A. Gupta, M. T. Swihart, and H. Wiggers, *Adv. Funct. Mater.* **19**, 696 (2009).
- <sup>13</sup>Z. C. Holman, C.-Y. Liu, and U. R. Kortshagen, *Nano Lett.* **10**, 2661 (2010).
- <sup>14</sup>S. Weis, R. Körmer, M. P. M. Jank, M. Lemberger, M. Otto, H. Ryssel, W. Peukert, and L. Frey, *Small* **7**, 2853 (2011).
- <sup>15</sup>R. N. Pereira, S. Niesar, W. B. You, A. F. da Cunha, N. Erhard, A. R. Stegner, H. Wiggers, M.-G. Willinger, M. Stutzmann, and M. S. Brandt, *J. Phys. Chem. C* **115**, 20120 (2011).
- <sup>16</sup>R. Lechner, H. Wiggers, A. Ebbers, J. Steiger, M. S. Brandt, and M. Stutzmann, *Phys. Status Solidi RRL* **1**, 262 (2007).
- <sup>17</sup>N. Petermann, N. Stein, G. Schierning, R. Theissmann, B. Stoib, M. S. Brandt, C. Hecht, C. Schulz, and H. Wiggers, *J. Phys. D* **44**, 174034 (2011).
- <sup>18</sup>S. Niesar, W. Fabian, N. Petermann, D. Herrmann, E. Riedle, H. Wiggers, M. S. Brandt, and M. Stutzmann, *Green* **1**, 339 (2011).
- <sup>19</sup>C.-Y. Liu, Z. C. Holman, and U. R. Kortshagen, *Nano Lett.* **9**, 449 (2009).
- <sup>20</sup>C.-Y. Liu, Z. C. Holman, and U. R. Kortshagen, *Adv. Funct. Mater.* **20**, 2157 (2010).
- <sup>21</sup>K.-Y. Cheng, R. Anthony, U. R. Kortshagen, and R. J. Holmes, *Nano Lett.* **11**, 1952 (2011).
- <sup>22</sup>K.-Y. Cheng, R. Anthony, U. R. Kortshagen, and R. J. Holmes, *Nano Lett.* **10**, 1154 (2010).
- <sup>23</sup>R. J. Anthony, D. J. Rowe, M. Stein, J. Yang, and U. Kortshagen, *Adv. Funct. Mater.* **21**, 4042 (2011).
- <sup>24</sup>A. R. Stegner, R. N. Pereira, R. Lechner, K. Klein, H. Wiggers, M. Stutzmann, and M. S. Brandt, *Phys. Rev. B* **80**, 165326 (2009).
- <sup>25</sup>R. N. Pereira, A. R. Stegner, T. Andlauer, K. Klein, H. Wiggers, M. S. Brandt, and M. Stutzmann, *Phys. Rev. B* **79**, 161304(R) (2009).
- <sup>26</sup>R. N. Pereira, A. J. Almeida, A. R. Stegner, M. S. Brandt, and H. Wiggers, *Phys. Rev. Lett.* **108**, 126806 (2012).
- <sup>27</sup>X. D. Pi, R. Gresback, R. W. Liptak, S. A. Campbell, and U. Kortshagen, *Appl. Phys. Lett.* **92**, 123102 (2008).
- <sup>28</sup>S. Niesar, R. N. Pereira, A. R. Stegner, N. Erhard, M. Hoeb, A. Baumer, H. Wiggers, M. S. Brandt, and M. Stutzmann, *Adv. Funct. Mater.* **22**, 1190 (2012).
- <sup>29</sup>R. N. Pereira, D. J. Rowe, R. J. Anthony, and U. Kortshagen, *Phys. Rev. B* **86**, 085449 (2012).
- <sup>30</sup>V. G. Kravets, C. Meier, D. Konjhodzic, A. Lorke, and H. Wiggers, *J. Appl. Phys.* **97**, 084306 (2005).
- <sup>31</sup>R. N. Pereira, D. J. Rowe, R. J. Anthony, and U. Kortshagen, *Phys. Rev. B* **83**, 155327 (2011).
- <sup>32</sup>A. R. Stegner, R. N. Pereira, K. Klein, R. Lechner, R. Dietmueller, M. S. Brandt, M. Stutzmann, and H. Wiggers, *Phys. Rev. Lett.* **100**, 026803 (2008).
- <sup>33</sup>A. R. Stegner, R. N. Pereira, K. Klein, H. Wiggers, M. Brandt, and M. Stutzmann, *Physica B* **401-402**, 541 (2007).
- <sup>34</sup>X. D. Pi, L. Mangolini, S. A. Campbell, and U. Kortshagen, *Phys. Rev. B* **75**, 085423 (2007).
- <sup>35</sup>S. Brunauer, P. Emmet, and E. Teller, *J. Am. Chem. Soc.* **60**, 309 (1938).
- <sup>36</sup>J. Knipping, H. Wiggers, B. Rellinghaus, P. Roth, D. Konjhodzic, and C. Meier, *J. Nanosci. Nanotechnol.* **4**, 1039 (2004).
- <sup>37</sup>S. Niesar, A. R. Stegner, R. N. Pereira, M. Hoeb, H. Wiggers, M. S. Brandt, and M. Stutzmann, *Appl. Phys. Lett.* **96**, 193112 (2010).
- <sup>38</sup>A. Stesmans, *Phys. Rev. B* **48**, 2418 (1993).
- <sup>39</sup>A. Stesmans and V. V. Afanasev, *Phys. Rev. B* **54**, R11129 (1996).
- <sup>40</sup>A. Stesmans, *Phys. Rev. B* **61**, 8393 (2000).
- <sup>41</sup>A. Stesmans, *J. Appl. Phys.* **88**, 489 (2000).
- <sup>42</sup>K. L. Brower, *Phys. Rev. B* **38**, 9657 (1988).
- <sup>43</sup>K. L. Brower, *Phys. Rev. B* **42**, 3444 (1990).
- <sup>44</sup>A. R. Wilkinson and R. G. Elliman, *Phys. Rev. B* **68**, 155302 (2003).

- <sup>45</sup>P. Gupta, V. L. Colvin, and S. M. George, *Phys. Rev. B* **37**, 8234 (1988).
- <sup>46</sup>H. Kim, T. Spila, and J. Greene, *Surf. Sci.* **490**, L602 (2001).
- <sup>47</sup>M. C. Flowers, N. B. H. Jonathan, Y. Liu, and A. Morris, *J. Chem. Phys.* **99**, 7038 (1993).
- <sup>48</sup>H. Kim, G. Glass, S. Y. Park, T. Spila, N. Taylor, J. R. Abelson, and J. E. Greene, *Appl. Phys. Lett.* **69**, 3869 (1996).
- <sup>49</sup>M. Stutzmann, J.-B. Chevrier, C. P. Herrero, and A. Breitschwerdt, *Appl. Phys. A* **53**, 47 (1991).
- <sup>50</sup>A. Stesmans, *J. Appl. Phys.* **92**, 1317 (2002).
- <sup>51</sup>R. Helms and E. Poindexter, *Rep. Prog. Phys.* **57**, 791 (1994).
- <sup>52</sup>D. Pierreux and A. Stesmans, *Phys. Rev. B* **66**, 165320 (2002).
- <sup>53</sup>K. L. Brower, *Phys. Rev. B* **33**, 4471 (1986).
- <sup>54</sup>A. Stesmans and G. Van Gorp, *Phys. Rev. B* **42**, 3765 (1990).